Journal of Applied Polymer Science

Structural characterization and electrical properties of carbon nanotubes/epoxy polymer composites

Sofia Boukheir,[1,2] Adél Len,[3,4] János Füzi,[3,4] Viktor Kenderesi,[3] Mohammed Essaid Achour,[2] Nándor Éber,[3] Luis Cadillon Costa,[5] Amane Oueriagli,[1] Abdelkader Outzourhit[1]

[1]Physics Department, Faculté des Sciences, Laboratoire LPSCM, Sémlalia, B.P. 2390, Marrakech 40000, Morocco
[2]Physics Department, Laboratoire LASTID, Faculté des Sciences, Université Ibn Tofail, B.P. 133, Kénitra 14000, Morocco
[3]Complex Fluids Department and Neutron Spectroscopy Department, Institute for Solid State Physics and Optics Wigner Research Centre for Physics Hungarian Academy of Sciences, P.O. Box 49, Budapest H-1525, Hungary
[4]Civil Engineering Department and Automation Department, Faculty of Engineering and Information Technology, University of Pécs, Boszorkány Str. 2, Pécs 7624, Hungary
[5]I3N and Physics Department, University of Aveiro, Aveiro 3810-193, Portugal
Correspondence to: M. E. Achour (E-mail: achour.me@univ-ibntofail.ac.ma)

ABSTRACT: The purpose of this study is to identify the relationship between the electrical and structural characteristics of multiwalled carbon nanotubes dispersed into the polymer matrix of a resin. In a first step, the composites were characterized by small-angle neutron scattering, which provide information about the bulk dispersion of nanotubes in the matrix and form three-dimensional networks with a surface fractal behavior. In the second step, a dielectric and electrical study was carried out in the frequency range between 1 Hz and 10 MHz at room temperature. We have found that the electric and dielectric behavior of these composites can be described by Jonscher's universal dielectric response. We show that the critical exponents describing the concentration dependence of the conductivity and the dielectric constant, obtained in the vicinity of the percolation threshold, are in good agreement with the theoretical values. © 2016 Wiley Periodicals, Inc. J. Appl. Polym. Sci. **2016**, *133*, 44514.

KEYWORDS: electrical properties; fractal structure; percolation; impedance spectroscopy; small angle neutron scattering

Received 12 June 2016; accepted 27 September 2016
DOI: 10.1002/app.44514

INTRODUCTION

The first polymer nanocomposites using carbon nanotubes (CNT) as filler were reported in the early 1990s. Since then a significant number of scientific reports have been published.[1,2] Unfortunately, CNT materials obtained from different producers often have different characteristics concerning the morphology of the agglomerates of nanotubes, their surface properties, the amount of impurities or defects; all these make the comparison of the results of different researchers difficult. The relevance of the fractal concept in the prediction of the physical properties of composites has been stressed before demonstrating that the fractal dimension is linked to the dielectric relaxation process[3,4]; a study of the correlation of the insulating-conducting transition of composite materials with the fractal dimension of the aggregates was investigated in some works.[4,5] In this article, we report on the percolating system of carbon-nanotubes-filled epoxy polymer composite, which was studied at room temperature, for filler concentrations below and above the critical percolation concentration. The dielectric response of these composites show a power law dependence with frequency, which was analyzed using Jonscher's universal dielectric response model.[6] The percolation model is commonly used to describe the DC and low-frequency AC behavior of composite materials.[7] According to this theory, the electrical conductivity and the dielectric permittivity are expressed by scaling laws in the vicinity of the threshold concentration of percolation.[8] The dispersion of nanotubes in the host matrices is usually investigated by scanning electron microscopy (SEM) of fractured surfaces or by transmission electron microscopy (TEM) of thin slices from the composite.[9] These methods provide partial, local information, and consequently, yield limited knowledge about the internal structure of the aggregates themselves. In this work, we used small angle neutron scattering (SANS), a well-recognized investigative method for characterizing the nanostructure of our material. It provides information on the distribution of the nanoscaled filler material, representative for the whole volume of the sample. Many researchers have employed SANS to characterize composite structures, to examine the fractal behavior at specific length scales and to study changes

in the structure with respect to processing variables.[10,11] Here, we have applied this technique to characterize CNT-reinforced epoxy composites, revealing a power law behavior with decay rates indicating a surface fractal behavior of the nanotubes dispersed in the polymer matrix.

An interesting result of this study is the agreement obtained in the determination of the fractal dimension of different concentrations of carbon-nanotubes-filled polymer composites by two different techniques: small angle neutron scattering and impedance spectroscopy. In particular, we point out that the multiwall carbon nanotubes, inserted in an epoxy resin, show fractal behavior on different scales, with similar parameters.

EXPERIMENTAL

Materials

Multiwalled carbon nanotubes (MWCNT) from Cheap-Tubes, USA Laboratories, have a diameter of the primary CNT about 50 nm, length in the range of 10 to 20 μm and purity higher than 95 wt %. They were dispersed in an insulating epoxy matrix DGEBA (diglycidylic ether of bisphenol A) with a density of 1.19 g cm^{-3}, DC conductivity of 1.4×10^{-14} S m^{-1} and a glass transition temperature of about 80°C. MWCNT were mixed with the epoxy in different concentrations (0.2%, 0.5%, 0.8%, 1.0%, 1.5%, 2.0%, 2.5%, 3.0%, and 5.0%), and stirred at room temperature, before adding 1% of hardener to make the mixture cohesive. Gelation took 5 min for each sample after pouring it into the mold. The samples were unmolded after a few hours; then they were left in rest for 24 h in order to reach a complete polymerization.

Experimental Procedures

Small Angle Neutron Scattering (SANS) Measurements. SANS spectra were collected using the Yellow Submarine (YS) small angle neutron scattering instrument and at the FSANS time of flight instrument located at the steady-state reactor of Budapest Neutron Centre. Yellow Submarine is equipped with a 64 × 64 cm^2 two-dimensional position sensitive BF_3 detector, while FSANS has a ^{3}He detector, with a pixel size of 0.8 × 0.8 mm^2. The scattering intensity $I(Q)$ was obtained as a function of the momentum transfer[12]:

$$Q = \frac{4\pi}{\lambda} \sin 2\theta \tag{1}$$

where 2θ is the scattering angle. The covered Q range was 0.003 to 0.020 $Å^{-1}$ for FSANS and 0.01 to 0.3 $Å^{-1}$ for YS. Raw data treatment included correction for beam attenuation (according to the measured sample thickness), background noise and detector pixel sensitivity. According to the Bragg law, the size d of the detected features in a SANS experiment is inversely proportional to Q according to[12]

$$d = \frac{2\pi}{Q} \tag{2}$$

thus large-scale structures will be visible at small Q. The upper limit in size is thus defined by the lowest Q value accessible to the experiment. The accessible size range for the FSANS instrument is 30 nm to 200 nm, and for the YS is 2 nm to 60 nm.

Scattering originates from the difference of the coherent neutron scattering densities (called contrast, K) of the two components, namely the polymer matrix and the nanotubes.

For discrete populations of isolated scattering objects with $Q R \ll 1$ (Guinier behavior), where R is the object radius, the scattered intensity is related to the radius of gyration of the object, R_g according to eq. (3)[12]:

$$\lim_{Q\to 0} I(Q) = A \exp\left(\frac{-Q^2 R_g^2}{3}\right) . \tag{3}$$

where A is proportional to the volume fraction of the scattering object (nanotube), and to the difference between the scattering length density of the polymer and that of the nanotube. R_g does not imply any assumption about the shape of the objects; however, the length of the nanotubes (in the range of microns) is outside of the detectable size range. Therefore we can only get information about the diameter of the CNTs.

According to Porod[13] and Debye,[14] the behavior of $I(Q)$ at Q tending to infinity is proportional to Q^{-4} in a system with smooth and clear interface between the scattering particles and the surrounding matrix:

$$\lim_{Q\to\infty} I(Q) = 2\pi S_V K^2 \left(\frac{1}{Q}\right)^4 + C, \tag{4}$$

where K is the previously mentioned scattering contrast within the sample that can be calculated from the chemical composition, S_V is the total scattering surface area per unit volume of the sample irradiated by the beam, and C is the incoherent background. Therefore, the scattering curve at large Q values ($Q \gg 1/R$) will depend only on the total scattering surface area per unit volume of the sample irradiated by the beam. In case of a distribution of sizes, S_V is an average, weighted towards the smaller particles. From these considerations it follows that in dense systems, within one scattering feature, in the limit of high Q, the scattering curve obeys the Porod law [eq. (4)][12] and the scattered intensity becomes proportional to the internal surface area of the scattering features per volume unit, thus the value of S_V can be obtained.

At large Q, a change in the slope of the SANS curve, plotted as log$I(Q)$ versus log$Q$, marks the boundary between different regimes, characterised by different length scales.

In general, the $I(Q)$ curve can be fitted in the large-Q-range with a power law similar to that in eq. (4):

$$\lim_{Q\to\infty} I(Q) = 2\pi S_V K^2 \left(\frac{1}{Q}\right)^p + C. \tag{5}$$

Here the exponent p depends on the structure of the scattering particles and on their mass or surface organisation. For example, if the structural features of a system are governed by a fractal arrangement (mass of surface fractals), instead of $p = 4$ the exponent p can take a non-integer value. For mass (or volume) fractals, the fractal dimension is[15]: $D = p$, $1 < p < 3$. For surface fractals, the fractal dimension is: $D_S = 6 - p$, $3 < p < 4$.

For scattering objects with smooth boundaries, but with a continuous change in the scattering density, the exponent p can also take values higher than 4.

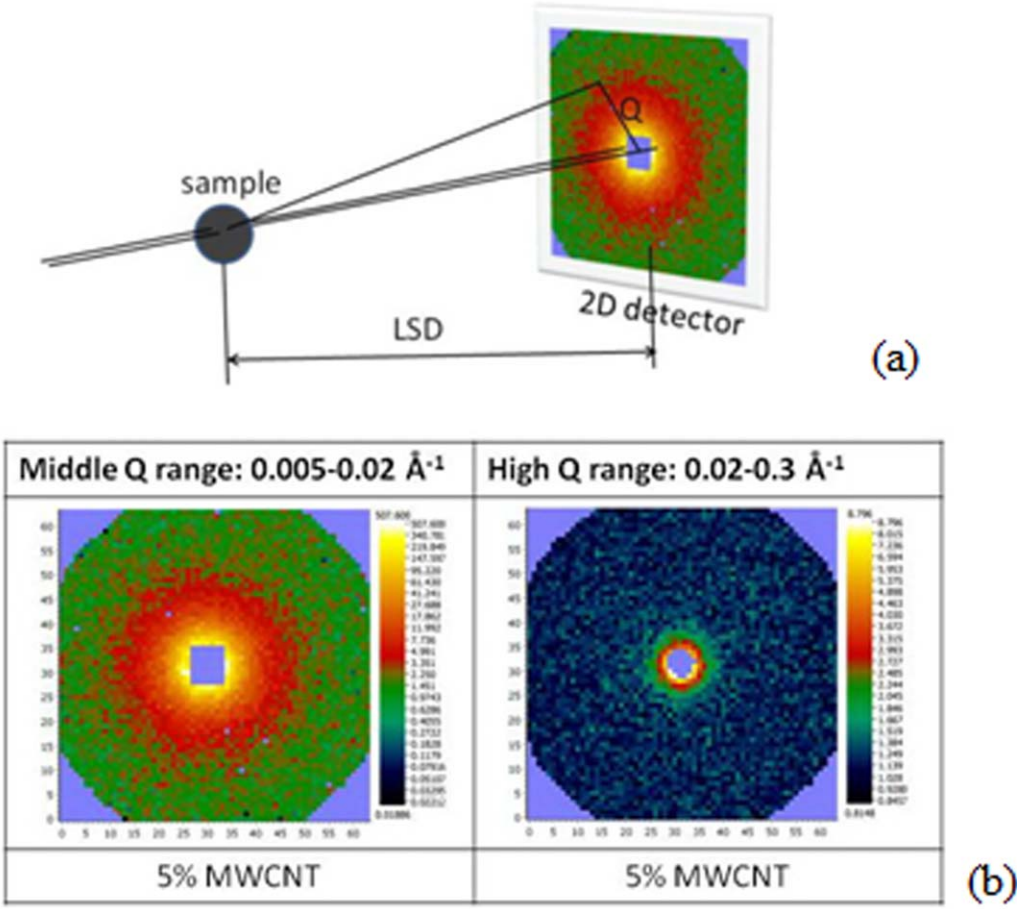

Figure 1. (a) The scattering geometry. (b) Two-dimensional images measured with the YS at the two different LSDs. [Color figure can be viewed at wileyonlinelibrary.com].

The measurements covered the overall Q range of 0.003 to 0.3 $Å^{-1}$; the sample to detector distances (LSD) for the YS were 1.3 m and 5.4 m; for the FSANS the LSD was 4 m. The YS used a fixed neutron wavelength of $\lambda = 4.88$ Å, while in the case of the FSANS, the wavelength varied between 3 Å and 10 Å.

For the used set-ups the instrumental resolutions (neglecting the gravitational effect) were $\sigma^2 = 2.8 \times 10^{-7} \pm 3.4 \times 10^{-6}$ $Å^{-2}$ for the FSANS, and $\sigma^2 = 8.7 \times 10^{-6} \pm 9.6 \times 10^{-4}$ $Å^{-2}$ for the Yellow Submarine.

Electrical Measurements. The temperature dependent AC impedance spectra were measured by using a Novocontrol Alpha-A Analyzer combined with the impedance interface ZG4, in the frequency range of 1 Hz $< f <$ 10 MHz. The complex permittivity $\varepsilon^* = \varepsilon' - i\,\varepsilon''$ was calculated; the dielectric constant ε' and the loss factor ε'' of the sample were deduced from the capacitance and the conductance, respectively. The samples were disks with 3 mm thickness and diameter of 12 mm. Each of the circular surfaces were polished and covered with a thin layer of silver to serve as electrode. ε' and ε'' were determined by non-linear mean square deviation curve fitting of the impedance spectrum using the WinFit program provided by Novocontrol, Hundsagen, Germany.[16] The estimated relative errors of σ_{AC}, ε' and ε'' are $\Delta\sigma_{AC}/\sigma_{AC} \leq 5\%$, $\Delta\varepsilon'/\varepsilon' \leq 5\%$ and $\Delta\varepsilon''/\varepsilon'' \leq 5\%$, respectively.[17]

RESULTS AND DISCUSSION

SANS Spectra

The scattering geometry and the two-dimensional (2D) scattering maps for the 5.0% MWCNT sample are shown in Figure 1(a,b), respectively. Figure 1(b) shows the detected 2D neutron intensities at two different Q ranges; the scattering is isotropic, thus the radial averaging of the 2D intensities measured at different Q ranges will give the overall one-dimensional (1D) SANS scattering curves.

Ten samples, measured on the YS (Figure 2) at large Q range (0.01–0.03 $Å^{-1}$), contained MWCNT of 0.0 to 5.0 wt % and showed power law exponents around $p2 = 3.67$. This value corresponds to a fractal-like behavior: the corresponding fractal dimension is equal to $D = 6 - p2 = 2.33$; it is characteristic to surface fractals, describing rough surfaces. Table I summarizes the power law exponents and the surface fractal dimensions of all samples measured at the YS.

Note, that the scattering from the 0.2% MWCNT sample in this Q range was comparable to the scattering from the polymer

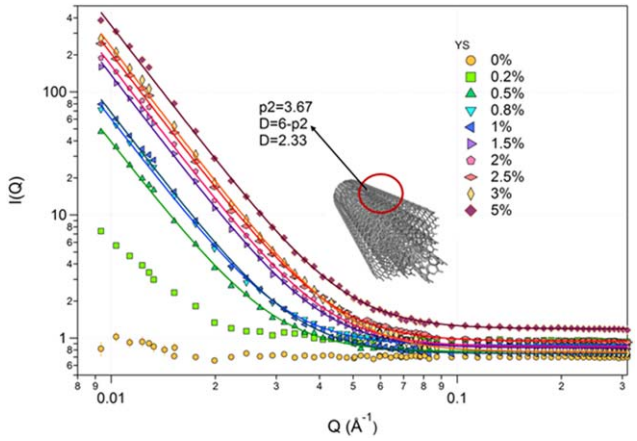

Figure 2. SANS scattering in the large Q range, measured on the YS. The symbols represent the measured values, the lines represent the fitted curves. [Color figure can be viewed at wileyonlinelibrary.com].

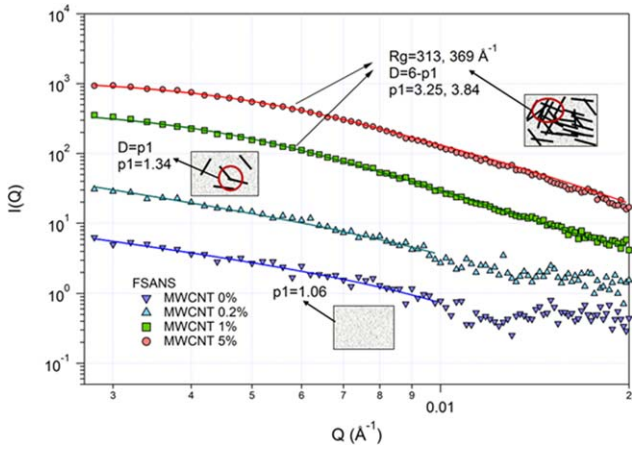

Figure 3. SANS scattering at small Q range, measured on FSANS. The symbols represent the measured values at FSANS, the lines represent the fitted curves. [Color figure can be viewed at wileyonlinelibrary.com].

matrix; therefore, at this concentration, a model fitting and the determination of $p2$ was not possible.

Four samples, containing 0.0%, 0.2%, 1.0%, and 5.0 weight % of MWCNT, were measured on the FSANS instrument too, in the small Q range (0.003–0.020 Å^{-1}, see Figure 3).

The samples with 1.0% and 5.0% MWCNT showed Guinier behavior, therefore a gyration radius R_g could be obtained from the fitting, yielding an average value around 60 nm for the diameter of the nanotubes. The fitting (see Figure 3) was made with a model combining eqs. (3) and (5):

$$I(Q) = A\exp\left(\frac{-Q^2R_g^2}{3}\right) + B\left(\frac{Q}{\mathrm{erf}\left(QR_g/\sqrt{6}\right)^3}\right)^{-p} \quad (6)$$

MWCNT, as seen by cold neutrons at small Q values, are one dimensional structures, showing power law scattering that, in case of completely dispersed and clean nanotubes, is expected to have a slope with $p = 1$.[9] The sample containing 0.2% CNT showed a slope of −1.34, which is close to the slope showed by the polymer matrix ($p = 1.06$). The difference is caused by the scattering coming from the nanotubes. We conclude that for the 0.2% sample, the dispersion of the CNT was much better, than in case of higher concentrations; thus neutron scattering occurred from either single or less aggregated nanotubes.

In the case of samples, where aggregation of the nanotubes is assumed, mass fractal behavior is expected in small Q range; that would evidence the presence of three-dimensional networks of nanotubes. However, the different size ranges cannot be sharply separated; the effect of the scattering from the surface of the nanotubes (seen by the YS) is present in this size range, too. This increases the value of the exponent p, and yields values characteristic of surface fractals: $p = 3.25$ and 3.84 for the 1.0% and 5.0% MWCNT containing samples, respectively. Therefore we conclude that in the bulk of all samples, but the one with 0.2% MWCNT content, the nanotubes form complex, three-dimensional networks, and their surface is characterized by surface fractal behavior.

Table I. Power Law Exponents and Fractal Dimensions of the Samples Measured on YS

Yellow submarine		
MWCNT concentration (%)	Exponent: $p2$	Fractal dimension: $D = 6 - p2$
0.2	—	—
0.5	3.64	2.36
0.8	3.67	2.33
1.0	3.69	2.31
1.5	3.67	2.33
2.0	3.68	2.32
2.5	3.67	2.33
3.0	3.68	2.32
5.0	3.65	2.35

Electrical Properties

The filler-concentration dependence of the electrical conductivity of the composite is characterized by a transition from insulating to conducting behavior, occurring at a critical concentration Φ_c. In agreement with the percolation theory, the electrical properties may exhibit a power law behavior in the neighborhood of Φ_c. It is important to emphasize that the AC conductivity and permittivity of percolating systems have been studied by using different physical models: the intercluster polarization model, the RC model,[18] and the anomalous diffusion model.[19] The total conductivity $\sigma_{tot}(\omega,T)$ at a given temperature T can be written as[20]:

$$\sigma_{tot}(\omega, T) = \sigma_{DC}(T) + \sigma_{AC}(\omega, T) \ (\omega = 2\pi f), \quad (7)$$

where $\sigma_{DC}(T)$ is the DC conductivity and $\sigma_{AC}(\omega,T)$ is the AC conductivity. The DC conductivity can be expressed theoretically as:

$$\sigma_{DC} \propto |\Phi - \Phi c|^t \quad \text{for } \Phi > \Phi c, \quad (8)$$

where Φ is the concentration of the filler and t is a critical exponent. The behavior of the dielectric constant ε' of those

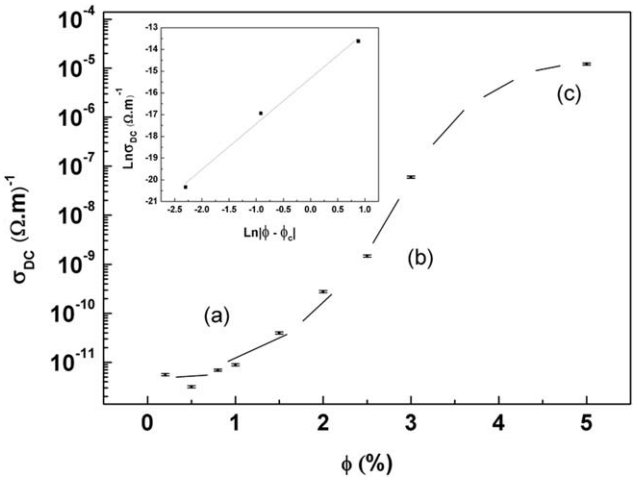

Figure 4. DC electrical conductivity σ_{DC} of the composite at constant temperature, as a function of the concentration Φ of the carbon nanotubes. The inset shows the logarithmic plot of DC conductivity versus $|\Phi - \Phi c|$ in the vicinity of the percolation threshold Φ_c.

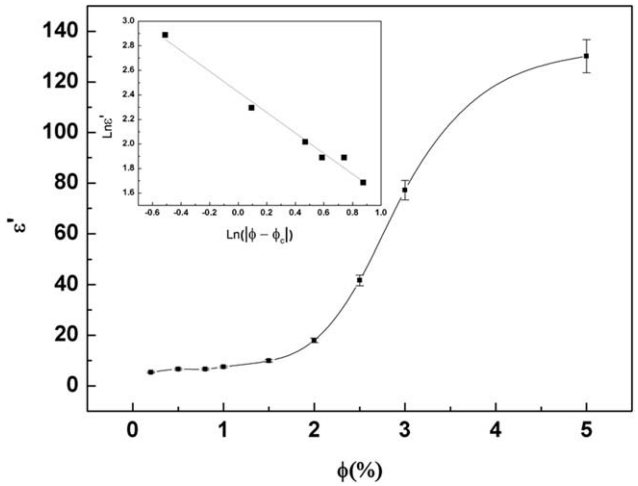

Figure 5. Dependence of the real part ε' of the permittivity on the concentration Φ of the carbon nanotubes at room temperature. The inset shows the logarithmic plot of ε' versus $|\Phi - \Phi c|$ in the vicinity of the percolation threshold Φ_c.

composite materials was also analyzed. The asymptotic behavior of ε' is given by:

$$\varepsilon' \propto |\Phi - \Phi c|^{-s} \quad \text{for } \Phi < \Phi c \ . \tag{9}$$

The exponents s and t characterize the divergence of ε' and σ_{DC} in the vicinity of Φ_c. Based on the general analytical properties of the complex permittivity of composites, Bergman and Imry[21] showed that the dielectric loss ε'' would also diverge near the percolation threshold and would follow a similar power law equation, though with a different critical exponent r. So ε'' obeys:

$$\varepsilon'' \propto |\Phi - \Phi c|^{-r}. \tag{10}$$

Figure 4 shows the MWCNT-concentration dependence of the DC conductivity for the composites at room temperature. The electrical percolation threshold is identified by a particular critical value Φ_c of the concentration, where the conductivity of the composite increases considerably. In our case, the percolation threshold was found at $\Phi_c = 2.7\%$. The concentration dependence of the conductivity can be divided into three regions (Figure 4). In region (a), a small number of charged particles are transporting current via a noncontinuous conductive path, which explains the small increase of the conductivity of the composite with Φ. With further increase of Φ, gradually, a continuous conductive path forms in the polymer matrix (i.e. a percolation occurs), yielding a sharp increase in the conductivity, as recognizable in region (b). In region (c), adding a further amount of filler has only a marginal effect on the conductivity and $\sigma_{DC}(\Phi)$ saturates. At this stage, the conductivity of the composite is controlled by the conducting filler particles.[22]

The variations of the dielectric constant ε' and the dielectric loss ε'' versus MWCNT concentration at low frequency, $f = 1$ Hz, are depicted in Figures 5 and 6, respectively. From the insets of these graphs, it is evident that ε' and ε'' variations are in agreement with the percolation theory, which predicts a divergence in the permittivity close to the percolation threshold.

The exponents t and s are assumed to be universal, i.e., they depend only on the dimensionality of the system. The theoretically predicted value of the exponent t is 2 and the typical experimental values are between 1.70 and 2.[23] Our measurements yielded the exponent $t = 2.10$ (see the inset in Figure 4). Numerical calculations by Straley,[24] for a medium made of cubic lattices of resistors, produced a critical exponent $s = 0.70 \pm 0.05$. Experimental data reported[25] for the exponent s in real media are typically in agreement with this value. For our case, the slope of $\ln\varepsilon'$ versus $\ln(\Phi - \Phi_c)$ yields the critical exponent $s = 0.84$ (see the inset in Figure 5). In the case of a perfect conductor dispersed in a perfect dielectric material, the three exponents t, s, and r are related by the relation[26]:

$$r = t + 2s \tag{11}$$

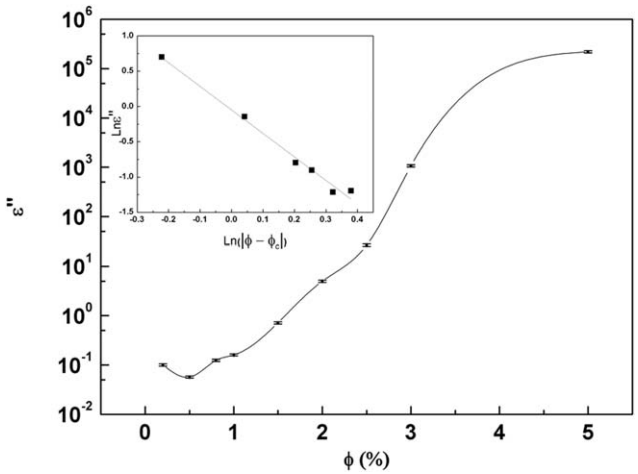

Figure 6. Dependence of the imaginary part ε'' of the permittivity on the concentration of the carbon nanotubes at room temperature. The inset shows the logarithmic plot of ε' versus $|\Phi - \Phi c|$ in the vicinity of the percolation threshold Φ_c.

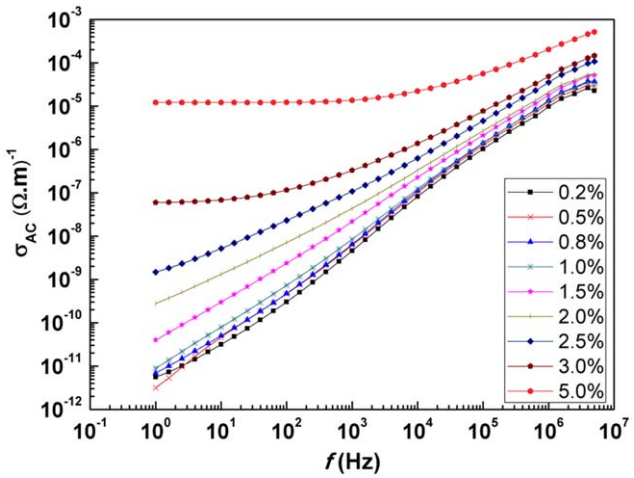

Figure 7. σ_{AC} versus frequency at room temperature for several carbon nanotube concentrations. [Color figure can be viewed at wileyonlinelibrary.com].

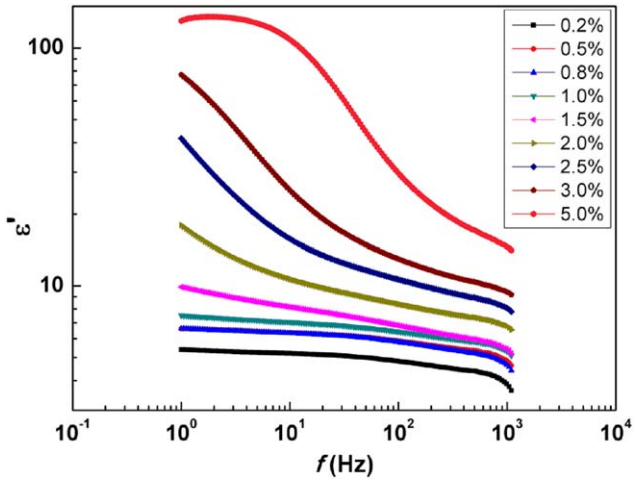

Figure 8. The real part ε′ of the complex permittivity of composites as a function of frequency, for different carbon nanotube concentrations, at room temperature. [Color figure can be viewed at wileyonlinelibrary.com].

The inset in Figure 6 shows the logarithmic plot of $\varepsilon''(\Phi - \Phi_c)$ for concentrations below Φ_c. The least-squares fitting yields $r = 3.33$, i.e., it is close to the value of 3.77 that is expected from eq. (11) using the values of t and s obtained from Figures 4 and 5.

Figure 7 shows the AC conductivity of the composite, as a function of the frequency, for different concentrations of MWCNT. The curves depict a monotonic increase of σ_{AC} with the frequency as well as with the concentration. We note that at low frequencies, for the concentrations above Φ_c, the AC conductivity is almost independent of the frequency; therefore $\sigma_{AC}(\omega)$ at low ω is identified as the DC conductivity. This behavior is observed up to an onset frequency, denoted as $f_c = \omega_c/2\pi$, at which the conductivity starts to increase with f (see also Figure 9). The frequency dependence of $\sigma_{AC}(\omega)$ in the high f, dispersive regions was analyzed using the power law[27]: $\sigma_{AC}(\omega) = A\,\omega^n$, where the exponent n is a temperature-dependent characteristic parameter, which measures the degree of interaction of mobile charges with the environment.[28] This behavior is characteristic of the charge transport in disordered materials and was interpreted by Jonscher[6] as a universal dynamic response. This electrical behavior is observed in materials of entirely different types, such as disordered semiconductors, polymers, conducting polymer compounds, ceramics, ion conducting glasses, heavily doped ionic crystals, etc. The dispersion region emerges from the DC conductivity plateau at the characteristic frequency (f_c) where the relaxation effects of the ions occur.[29] This characteristic frequency is, however, a not well-defined material parameter; it depends upon many factors, such as the method of the synthesis, microstructure formation, composition, etc.[30] Experimentally, it can be obtained as an intersection of the straight lines fitted to the plateau at $f < f_c$ and the slope of $\sigma_{AC}(\omega)$ for $f > f_c$, respectively (see the upmost graph in Figure 9). In our case, f_c was localized as the frequency, where $\sigma_{AC}(\omega_c) = 1.1\ \sigma_{DC}$. The exponent n was measured as the slope of the high frequency region $f > f_c$ for the concentrations above Φ_c, otherwise (i.e. for $\Phi < \Phi_c$), the slope was taken for the whole frequency range (see the spectra in Figure 7). We found n values ranging between 0.84 and 0.94, as reported in Table II. According to Kilbride *et al.*[31] a power law with $0.8 < n < 1.0$ is characteristic of the hopping in a disordered material, where the hopping charge carriers are subject to energy barriers varying spatially randomly.

In Figure 8 the real part ε′ of the complex permittivity is plotted versus the frequency, for different concentrations of carbon nanotubes, at room temperature. The curves exhibit a dispersion (a decrease of ε′ with increasing f). The enhanced dispersion with increasing MWCNT concentration is attributed to the increase of σ_{DC}.

Fractal Model of Dielectric Relaxation

As pointed out in the Introduction, the dielectric relaxation phenomena of the composites are subjected to Jonscher's universal dielectric response model,[6] which yields a power law dependence of the permittivity on the frequency.[25] If the system has a fractal behavior, the exponents are related to the fractal dimensions. In this section, we consider two cases of

Table II. Power Law Exponents of the Samples Measured on YS and Calculated from Permittivity Results

Φ (%)	0.2	0.5	0.8	1.0	1.5	2.0	2.5	3.0
n	0.94	0.94	0.94	0.94	0.92	0.91	0.88	0.84
D_f (from permittivity)	2.89	2.89	2.87	2.88	2.83	2.82	2.77	2.69
D_f (from SANS)	2.36	2.33	2.31	2.33	2.32	2.33	2.32	2.35

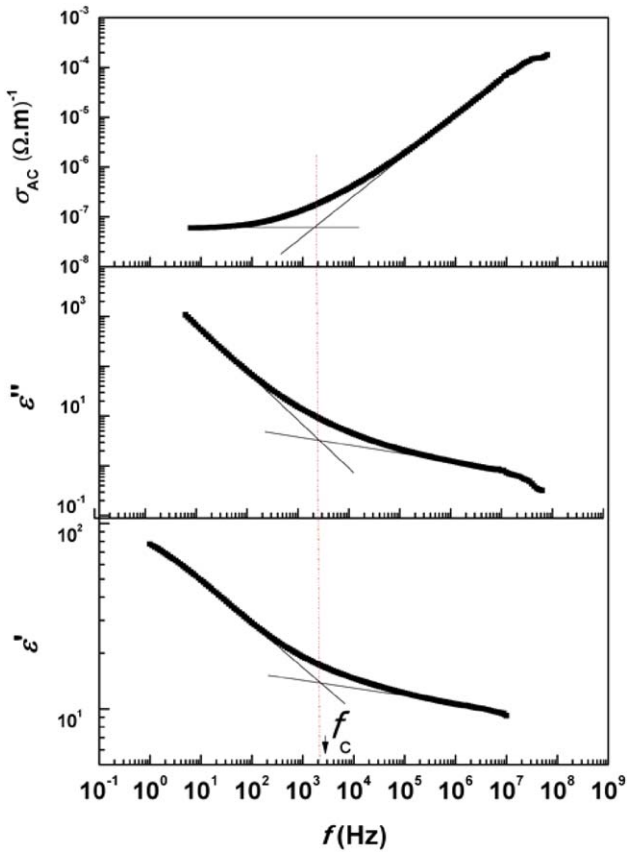

Figure 9. Frequency dependence of ε', ε'', and σ_{AC} (logarithmic scales), at the concentration of $\Phi = 3.0\%$ and $T = 25\,^{\circ}C$. [Color figure can be viewed at wileyonlinelibrary.com]

conduction in fractal systems: conduction on fractal aggregates and conduction at fractal surfaces.

In the case of conduction on fractal aggregates, from the point of view of the electrical conductivity, the composite may be regarded as a medium with a fractal structure.[32] If the Brownian movement of charge carriers takes place over such a fractal structure, the temporal evolution of the length $L(t)$ covered by the charge carriers scales with time through the fractal dimension D_w as[32]:

$$L(t) \propto t^{1/D_w} \propto \omega^{-1/D_w}, \tag{12}$$

where D_w is the fractal dimension of the movement of charge carriers with $1 < D_w < 2$. According to the Einstein diffusion equation, the diffusion coefficient $M(\omega)$ can be written, by using eq. (12), as:

$$M(\omega) \propto \frac{L^2(t)}{t} \propto \omega L^2\ (\omega) \propto \omega^{1-2/D_w}. \tag{13}$$

The conductivity provided by the charge carriers is related to the Brownian movement, therefore the AC conductivity taking place in the fractal structure obeys then the following law:

$$\sigma_{AC}(\omega) \propto (L(\omega))^{D_f-2}\ M(\omega), \tag{14}$$

where the fractal dimension of the structure, D_f, satisfies $2 < D_f < 3$. Then, substituting eq. (13) into eq. (14), we obtain:

$$\sigma_{AC}(\omega) \propto \omega^{1-\frac{D_f}{D_w}} = \omega^n \text{ with } n = 1 - \frac{D_f}{D_w}. \tag{15}$$

If, however, the conduction occurs at the fractal surfaces (the charge transport takes place as a diffusive process in the fractal interface, which can be considered as a bidimensional discontinuity), the frequency scaling of the conductivity changes. According to Niklasson,[32] under such conditions the power law still remains, but with a different exponent. Thus for conduction at the fractal surface one obtains:

$$\sigma_{AC}(\omega) \propto \omega^n \text{ with } n = \frac{D_f - 1}{2}. \tag{16}$$

In materials, which exhibit a negligible DC conductivity at low frequencies and where the previous behavior—eq. (16)—is realized, the following empirical relations can be established for the behavior of the dielectric permittivity[3]:

$$\varepsilon'(\omega) \propto \varepsilon''(\omega) \propto \omega^{n-1} \quad \text{for } f > fc\ . \tag{17}$$

As an example, Figure 9 exhibits the frequency dependent $\varepsilon'(\omega)$, $\varepsilon''(\omega)$, and $\sigma_{AC}(\omega)$ for the sample with 3% of MWCNT. As already mentioned before, the crossover frequency f_c is obtained as the intersection of the horizontal DC line of $\sigma_{AC}(\omega)$ with the extrapolated constant-slope part of the curve above the first inclination point, where the "power-law" behavior begins to be observed (see the upper panel of Figure 9). It can be seen, however, that the slope of the $\varepsilon'(\omega)$ and $\varepsilon''(\omega)$ curves also changes at f_c (see the lower and middle panels of Figure 9, respectively); thus they can also be used for determining the crossover frequency.

The SANS measurement reported above uncovered the surface fractal behavior of the composites. Therefore, at calculating the fractal dimension D_f of the composites with various carbon nanotube concentrations from the dielectric permittivity results, eqs. (16) and (17) should be applied; hence $D_f = 2n + 1$.[33]

Table II summarizes the values of exponent n and the fractal dimensions D_f, firstly, obtained from the permittivity results and secondly, determined by the small angle neutron scattering measurements. One can notice that the dimensionality parameters yielded by the dielectric permittivity measurements are closer rather to 3 than 2; they are higher than the dimension of a surface and lower than a volume dimension. This may be because the geometrical features of the carbon nanotubes are not the only ones governing the structure of the clusters of primary aggregates; the chemical surface properties should also have an important role.[4]

CONCLUSIONS

This work allowed us to explore the low frequency dielectric behavior of heterogeneous materials composed of carbon nanotubes in an epoxy resin. We found that the dielectric response of these composite materials change significantly at the percolation transition. We learned that the dielectric behavior of these composites can be described by Jonscher's universal dielectric response. We showed that the critical exponents describing the concentration dependence of the conductivity and the dielectric constant, obtained near the percolation threshold, are in good agreement with previously published values. As for

characterizing the composites by neutron scattering, we proved that the nanotubes form three-dimensional networks; thus the aggregation of the nanotubes inside the epoxy resin matrix was evidenced. In the Q range seen by small angle neutron scattering, the surface of the nanotubes is rough (surface fractal behavior), which can be attributed to the imperfections of their surface, and to the presence of carbon clusters, pores, or additives on the surface. At lower nanotube concentration the dispersion was found to be better. The average diameter of the nanotubes inside the epoxy matrix was found to be around 60 nm.

Analysis of the AC electrical conductivity of the carbon-nanotubes-filled polymer samples uncovered a fractal behavior with similar dimensionality as that obtained by neutron scattering. This interesting agreement, which was found despite of the difference in the length scales accessed by the two techniques, represent a first, but necessary step in understanding the role of fractals in describing the structure and predicting the physical properties of carbon-nanotubes-containing composite materials. Though the existence of a relation between the morphology of carbon nanotubes and the physical properties of the composite materials, which contain them, has been reported before, there are still many unsolved questions, e.g., concerning the correlation between fractal parameters and the percolation treshold of CNT-based nanocomposites, which will be in the focus of further experimental studies.

ACKNOWLEDGMENTS

Financial support by the Moroccan (CNRST)–Hungarian (NKFIH) bilateral project TÉT_12_MA-1-2013-0010 and the Budapest Neutron Centre (www.bnc.hu) are gratefully acknowledged. Authors also thank FEDER funds through the COMPETE 2020 Programme and National Funds through FCT—Portuguese Foundation for Science and Technology under the project UID/CTM/50025/2013.

REFERENCES

1. Ramasubramaniam, R.; Chen, J.; Liu, H. *Appl. Phys. Lett.* **2003**, *83*, 2928.
2. Allaoui, A.; Bai, S.; Cheng, H. M.; Bai, J. B. *Compos. Sci. Technol.* **2002**, *62*, 1993.
3. Niklasson, G. A. *Phys. D* **1989**, *38*, 260.
4. Salome, L.; Carmona, F. *Carbon* **1991**, *29*, 599.
5. Alig, I.; Pötschke, P.; Lellinger, D.; Skipa, T.; Pegel, S.; Kasaliwal, G. R.; Villmow, T. *Polymer (Guildf)* **2012**, *53*, 4.
6. Jonscher, A. K. *IEEE Trans. Electron. Insul.* **1992**, *27*, 407.
7. Kyrylyuk, A. V.; van der Schoot, P. *Proc. Natl. Acad. Sci. USA* **2008**, *105*, 8221.
8. Achour, M. E.; Droussi, A.; Zoulef, S.; Gmati, F.; Fattoum, A.; Belhadj Mohamed, A.; Zangar, H. *Spectrosc. Lett.* **2008**, *41*, 299.
9. Koszor, O.; Tapasztó, L.; Markó, M.; Balázsi, C. *Appl. Phys. Lett.* **2008**, *93*, 2006.
10. Jouault, N.; Dalmas, F.; Sylvère, S.; Di Cola, E.; Schweins, R.; Jestin, J.; Boué, B. *Phys. Rev. E* **2010**, *82*, 031801.
11. Hopkins, A. R.; Tomczak, S. J.; Vij, V.; Jackson, A. *J. Thin Solid Films* **2011**, *520*, 1617.
12. Glatter, O.; Kratky, O. Small-Angle X-ray Scattering, Academic Press, London, **1982**.
13. Porod, G. *Kolloid Z* **1951**, *124*, 83.
14. P. Debye, A. B. *Appl. Phys.* **1949**, *20*, 518.
15. Ficker, T.; Len, A. *J. Phys. D: Appl. Phys.* **2007**, *40*, 4055.
16. Novocontrol WinFIT Software. http://www.novocontrol.de/html/winfit.htm, (Accessed June 2016).
17. Samir, Z.; El Merabet, Y.; Graça, M. P. F.; Soreto Teixeira, S.; Achour, M. E.; Costa, L. C. *Polym. Compos.* **2016**, Doi: 10.1002/pc.24067.
18. Efros, A. L.; Shklovskii, B. I. *Phys. Status Solidi B* **1976**, *76*, 475.
19. Kochetov, R.; Andritsch, T.; Morshuis, P. H. F.; Smit, J. *J. IEEE Trans. Dielectr. Electron. Insul.* **2012**, *19*, 107.
20. Salman, F. *Turk. J. Phys.* **2004**, *28*, 41.
21. Bergman, D. J.; Imry, Y. *Phys. Rev. Lett.* **1977**, *39*, 1222.
22. Costa, L. C.; Achour, M. E.; Graça, M. P. F.; El Hasnaoui, M.; Outzourhit, A.; Oueriagli, A. *J. Non-Cryst. Solids* **2010**, *356*, 270.
23. Foulger, S. H. *J. Polym. Sci. Part B: Polym. Phys.* **1999**, *37*, 1899.
24. Straley, J. In AIP Conference Proceeding, Columbus, OH, September 1977; Garland, J.C., Tanner D.B., Eds.; American Institute of Physics: New York; 1978, Vol. 40, p 118.
25. Achour, M. E.; Brosseau, C.; Carmona, F. *J. Appl. Phys.* **2008**, *103*, 1.
26. Brosseau, C.; Achour, M. E. *J. Appl. Phys.* **2009**, *105*, 1.
27. Jonscher, A. K. *J. Phys. D: Appl. Phys.* **1999**, *32*, R57.
28. Chin, R. H.; Chang, R. Y.; Shern, C. S.; Fukami, T. *J. Phys. Chem. Solids* **2003**, *64*, 553.
29. Gjorgjevich, M. P.; Aleksovska, S.; Dimitrovska-Lazova, S. *Phys. Maced.* **2012**, *61*, 27.
30. Ravikiran, Y. T.; Lagare, M. T.; Sairam, M.; Mallikarjuna, N. N.; Sreedhar, B.; Manohar, S.; MacDiarmid, A. G.; Aminabhavi, T. M. *Synth. Met.* **2006**, *156*, 1139.
31. Kilbride, B. E.; Coleman, J. N.; Roth, S. *J. Appl. Phys.* **2002**, *92*, 4024.
32. Niklasson, G. A. *J. Phys: Condens. Matter* **1993**, *5*, 4233.
33. Lira-Olivares, J.; Marcano, D.; Lavelle, C.; Sánchez, F. G. *Rev. Latinoam. Metal. Y Mater.* **2000**, *20*, 68.